

The discovery of differential radial rotation in the pulsating subdwarf B star KIC 3527751

H. M. Foster and M. D. Reed

Department of Physics, Astronomy, and Materials Science, Missouri State University, Springfield, MO 65897

J. H. Telting

Nordic Optical Telescope, Rambla José Ana Fernández Pérez 7, 38711 Breña Baja, Spain

R. H. Østensen

Instituut voor Sterrenkunde, KU Leuven, Celestijnenlaan 200 D, 3001 Leuven, Belgium

A. S. Baran

Uniwersytet Pedagogiczny, Obserwatorium na Suhorze, ul. Podchorążych 2, 30-084 Kraków, Poland

ABSTRACT

We analyze three years of nearly-continuous *Kepler* spacecraft short cadence observations of the pulsating subdwarf B star KIC 3527751. We detect a total of 251 periodicities, most in the g -mode domain, but some where p -modes occur, confirming that KIC 3527751 is a hybrid pulsator. We apply seismic tools to the periodicities to characterize the properties of KIC 3527751. Techniques to identify modes include asymptotic period spacing relationships, frequency multiplets, and the separation of multiplet splittings. These techniques allow for 189 (75%) of the 251 periods to be associated with pulsation modes. Included in these are three sets of $\ell = 4$ multiplets and possibly an $\ell = 9$ multiplet. Period spacing sequences indicate $\ell = 1$ and 2 overtone spacings of 266.4 ± 0.2 and 153.2 ± 0.2 seconds, respectively. We also calculate reduced periods, from which we find evidence of trapped pulsations. Such mode trappings can be used to constrain the core/atmosphere transition layers. Interestingly, frequency multiplets in the g -mode region, which sample deep into the star, indicate a rotation period of 42.6 ± 3.4 days while p -mode multiplets, which sample the outer envelope, indicate a rotation period of 15.3 ± 0.7 days. We interpret this as differential rotation in the radial direction with the core rotating more slowly. This is the first example of differential rotation for a subdwarf B star.

Subject headings: stars: horizontal-branch — stars: individual (KIC 3527751) — stars: oscillations — stars: rotation — subdwarfs

1. Introduction

The *Kepler* spacecraft was launched in 2009 with a primary goal: to discover extrasolar planets by means of detecting their transits. To this end, the spacecraft has accomplished its mission; at the time of writing, Tenenbaum et al. (2014)

suggest there may be 16 285 potential stars with transit or eclipse detections.

Kepler's applications are broader than just hunting for extrasolar planets. The spacecraft has also been extremely useful for discovering binary stars, which allow us to derive the bulk characteristics of stars, such as mass, radius, distance, and

luminosity (Conroy et al. 2014). *Kepler* has also advanced the field of asteroseismology, or the process of using a star’s vibrations to determine its physical characteristics. *Kepler’s* Earth-trailing orbit allows it to continuously obtain data, avoiding ground-based limitations, such as daytime gaps, atmospheric transparency variations, and annual visibility cycles. *Kepler* only ceased observing during monthly data transmissions and a few safing events over the course of its four-year program.

Despite asteroseismology being a secondary goal, *Kepler* has been particularly successful for studying the oscillations of subdwarf B (sdB) stars. Subdwarf B stars are extreme horizontal branch stars with temperatures in the range of 20 000 to 40 000 K. These stars have shed their outer layers near the tip of the red giant branch and have become the exposed cores of horizontal branch stars (for a review of the properties of sdB stars see Heber 2009). The pulsations of sdB stars are divided into two categories based on their periods. Short period pressure (p -)mode pulsators, or V361 Hya stars, have amplitudes typically less than 1% of their mean brightness and pulsation periods of just a few minutes. Long period gravity (g -)mode pulsators are classified as V1093 Her stars with typical amplitudes below 0.1% and longer pulsation periods typically near an hour. Some stars exhibit both kinds of pulsation. These hybrids usually exhibit one pulsation type more strongly than the other, with one exception; KIC 9472174 which shows an abundance of both types of pulsation modes (Østensen et al. 2010a). The two classes are also separated in temperature with the V1093 Her stars being cooler than the V361 Hya stars (for a review of sdB pulsation properties, see Østensen 2010). In this paper we use the term sdBV to generically indicate pulsating sdB stars.

Kepler’s nearly-continuous observations have been particularly useful for the study of the longer period g -mode pulsators, for which ground-based data have not provided seismic solutions. At the time of writing, 17 papers have been published using *Kepler* observations of sdBV stars. Previously published results using *Kepler* data include the discovery of nearly-evenly-spaced g -mode periods (Reed et al. 2011) and the detection of frequency multiplets (Baran et al. 2012; Telting et al. 2012;

Østensen et al. 2012, 2014b; Reed et al. 2014), both of which can be used to identify pulsation modes. Asteroseismic rotation periods have been found to be on the order of tens to a hundred days. This includes binary stars which have been shown to be subsynchronous rotators, even with orbital periods as short as half a day (Pablo et al. 2011, 2012; Telting et al. 2012, 2014; Østensen et al. 2014b).

The objective of this or any other asteroseismological study is to characterize the physical properties of the star in question. Model constraints include spectroscopic measurements (T_{eff} and $\log g$), as well as asteroseismic properties. Asteroseismic constraints can be as simple as a list of frequencies to compare with models (as in the papers by Van Grootel et al. 2010; Charpinet et al. 2011b, using survey-phase *Kepler* data), or quite detailed, as in small structures in Echelle diagrams. Tools which have been applied to sdBV stars with some success include measuring stellar rotation via frequency multiplets (e.g. Telting et al. 2012); period spacings for mode identification (e.g. Reed et al. 2011); long overtone sequences observed in Echelle diagrams (e.g. Reed et al. 2014), as well as small deviations (e.g. Baran & Winans 2012); regions above and below which period spacings do not behave asymptotically; reduced period diagrams for detecting trapped modes (Østensen et al. 2014b); and sliding Fourier Transforms (sFTs) to resolve amplitude variations (Telting et al. 2012; Reed et al. 2014).

The target of this paper, KIC 3527751, was examined in a preliminary study of hybrid sdB pulsators by Reed et al. (2010). They detected 41 g - and 3 p -mode periodicities from one-month of *Kepler* survey data. 34 of the g -modes were identified as $\ell = 1$ or 2 using period spacings. Subsequent to *Kepler’s* survey phase, KIC 3527751 was continuously observed with one minute cadence from quarter 5 (Q5) until mission end during Q17. Here we analyze all available data (1148 days), providing our best estimate of the frequency content to which we apply our asteroseismological tools, as discussed above.

2. Data Analysis

Kepler obtains data in two modes: short cadence (SC), which produces one integration ev-

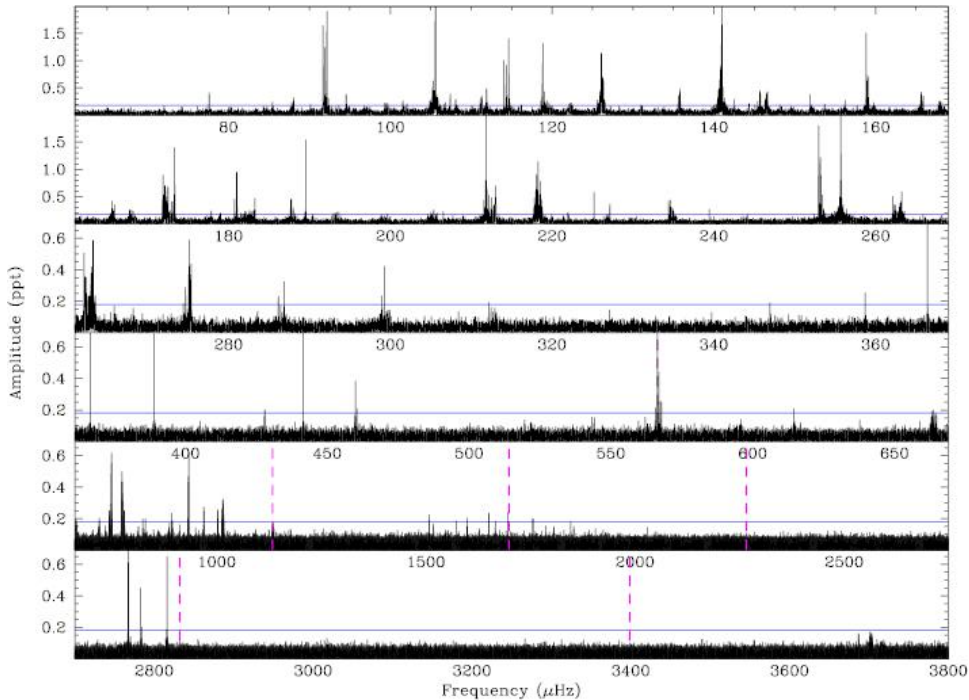


Fig. 1.— Fourier transform of KIC 3527751. The solid (blue) horizontal line is the 5σ detection limit and the dashed (magenta) vertical lines indicate known frequencies where spacecraft artifacts may occur.

ery 58.85 seconds, and long cadence (LC), which produces an integration every 30 minutes. Short cadence observations consume more of *Kepler's* limited memory, so the targets observed in this mode are far fewer. We downloaded optimally-extracted lightcurves from the Mikulski Archive for Space Telescopes¹, removed long-term trends (> 1.5 days) with low-order spline fitting, and normalized the data by mean brightness. We sigma-clipped the data at 5σ and multiplied the modulation intensities so amplitudes would appear in the Fourier transform (FT) as parts-per-thousand (ppt).

The data span almost 1148 days and include 1.55 million data points which is a temporal resolution of $0.010 \mu\text{Hz}$. These data have a duty cycle of 92.4%, with the largest gaps caused by spacecraft safing events during Q8, Q14, and Q16. As noted by Østensen et al. (2014a), a 4σ detection limit would contain ~ 50 spurious peaks, so we increased our detection limit to 5σ , to be reasonably confident that detections are real signal.

¹<http://archive.stsci.edu/kepler/>

We determined the mean level in the FT to be $\sigma_{FT} = 0.032 \text{ ppt}$, making our 5σ limit 0.16 ppt . It should be noted that a 5σ detection limit only applies when examining the entire FT. When looking for predicted periodicities in smaller regions (of, say a few hundred μHz), a 4σ detection limit is perfectly justified. Significant peaks range from 72 to $3704 \mu\text{Hz}$, though they are concentrated between $100 - 300 \mu\text{Hz}$. Peaks occurring below $20 \mu\text{Hz}$ are attributed to residual signal from the spacecraft which was not removed by our detrending. An FT of the data is shown in Fig. 1 with the detection limit indicated by a horizontal line.

As discussed in Reed et al. (2014), the previously utilized method of fitting the original lightcurve with a non-linear least-squares program and prewhitening the resulting Fourier transform (FT) would have been not only tedious, but rather counterproductive as exceptionally few peaks could be cleanly removed. We attribute this property to the long-term instability of amplitudes and even, occasionally, of frequencies. In order to evaluate the pulsation content, we used the two tools described in Reed et al. (2014): sliding FTs

(sFTs) to evaluate the pulsation content in the time domain and Lorentzian peak fitting which serves as a method for determining peak widths as an indicator of frequency errors.

Frequency multiplets are readily apparent in the FT (see Fig. 3) of the complete data set and were used as a guide for the sFTs. Sliding FTs were generated using data spanning 220 days, to fully resolve frequency multiplets, and stepped by 5 days through the entire data set. Sample sFTs are shown in Fig. 2 with sFTs of the entire frequency spectrum available on-line. The sFTs were used as guides for the Lorentzian fitting. If amplitudes were only detectable during a portion of the data, Lorentzian fits were obtained from only those portions (using data spanning a minimum of 200 days to insure frequencies are resolved). In total, we fitted 251 frequencies, which were compared with known spacecraft artifacts to ensure none are in our list (except f_{159} as noted in §3.1). Table 1 provides the pulsation frequencies, Lorentzian widths, and amplitudes resulting from our FT fitting.

2.1. Combination frequencies

A search for combination frequencies and a likelihood comparison was completed as in Telting et al. (2012). Residuals were calculated using the form $\delta f = f_3 - f_2 - f_1$ for all combinations of frequencies and those with $\delta f = 0$ within the errors were reported for examination. Eight combinations were discovered having $\delta f < 0.0001 \mu\text{Hz}$. Of these, three only involve low-amplitude frequencies which are unlikely to produce combination modes, while five have at least one higher-amplitude frequency. We consider it likely that these five actually are combination frequencies and they are listed in Table 2 and marked in Table 1 with asterisks.

2.2. Spectroscopy

Over the 2010 and 2011 observing seasons of the *Kepler* field, we obtained a total of 24 spectra of KIC 3527751. Low-resolution spectra ($R \approx 2000$ –2500) have been collected using the Kitt Peak 4-m Mayall telescope with RC-Spec/F3KB, the kpc-22b grating and a 1.5–2.0 arcsec slit, the 2.56-m Nordic Optical Telescope with ALFOSC, grism #16 and a 0.5 arcsec slit, and the 4.2-m William

Herschel Telescope with ISIS, the R600B grating and 0.8–1.0 arcsec slit. Exposure times were 600 s at KP4m and WHT, and either 500 s or 300 s at the NOT. The resulting resolutions based on the width of arc lines is 1.7 \AA for the KP4m and WHT setups, and 2.2 \AA for the setup at the NOT. See Table 3 for an observing log.

The data were homogeneously reduced and analysed. Standard reduction steps within IRAF include bias subtraction, removal of pixel-to-pixel sensitivity variations, optimal spectral extraction, and wavelength calibration based on arc-lamp spectra. To fully account for the blue CCD etching pattern in the NOT spectra, spectroscopic flats were constructed by interpolating between UVB imaging flats along the dispersion direction, as halogen flats suffered from stray light in the blue part of the spectrum. The target spectra and the mid-exposure times were shifted to the barycentric frame of the solar system. The spectra were normalised to place the continuum at unity by comparing with a model spectrum for a star with similar physical parameters as we find for the target (described below).

Radial velocities were derived with the FXCOR package in IRAF. We used the $H\gamma$, $H\delta$, $H\zeta$ and $H\eta$ lines to determine the radial velocities (RVs), and used the spectral model fit (described below) as a template. See Table 3 for the results, with errors in the radial velocities as reported by FXCOR. The errors reported by FXCOR are correct relative to each other, but may need scaling depending on, amongst other things, the parameter settings and the validity of the template as a model of the star.

We find that the RV data has more scatter than one would assume for a non-variable star, but that the RV data are not sufficient to constrain any orbital parameters. Excluding the datapoint from the worst S/N spectrum, the average $RV = -13.0 \pm 3.2 \text{ km s}^{-1}$, with an RMS scatter of 15.1 km s^{-1} which is much larger than the errors in the data that range from 3–13 km s^{-1} , with median individual error of 7.8 km s^{-1} . An FT gives maximum amplitude of 22 km s^{-1} in the frequency range of 0–17.4 μHz , and lower amplitudes at higher frequencies.

As in our previous papers (e.g. Østensen et al. 2010b), we have fitted the average spectrum from each observatory to model grids, in order to de-

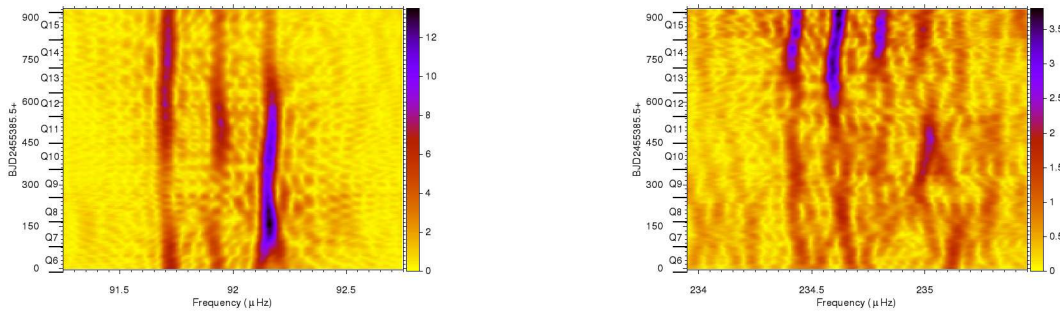


Fig. 2.— Examples of sliding Fourier transforms (sFTs). A complete set is available in the on-line material.

TABLE 1

TABLE OF ASTEROSEISMIC QUANTITIES. COLUMN 1 PROVIDES A LABEL FOR THE PERIODICITY, COLUMNS 2 AND 3 THE FREQUENCY AND PERIOD, WITH ERRORS IN PARENTHESES, AND COLUMN 4 THE OBSERVED AMPLITUDE TAKEN FROM THE LORENTZIAN FIT OF THE ENTIRE DATA SET. COLUMNS 5 THROUGH 8 PROVIDE OUR BEST ESTIMATE MODE IDENTIFICATIONS, COLUMNS 9 AND 10 PERIOD SPACING DEVIATIONS, AND COLUMN 11 THE FREQUENCY SPLITTING (FROM THE SUBSEQUENT FREQUENCY) OF MULTIPLET MEMBERS. [†] INDICATES PERIODICITIES DETECTED BY REED ET AL. (2010) AND * INDICATES FREQUENCIES WHICH ARE LISTED IN TABLE 2 AS PART OF A COMBINATION FREQUENCY. TABLE 1 IS PUBLISHED IN ITS ENTIRETY IN THE ELECTRONIC EDITION OF THE ASTROPHYSICAL JOURNAL. A PORTION IS SHOWN HERE FOR GUIDANCE REGARDING ITS FORM AND CONTENT.

ID	Freq. μHz	Period sec.	Amp. ppt	ℓ ...	m ...	$n_{\ell=1}$...	$n_{\ell=2}$...	$(\frac{\Delta P}{P})_{\ell=1}$...	$(\frac{\Delta P}{P})_{\ell=2}$...	δf μHz
f010	91.703 (0.008)	10904.73 (0.91)	1.64	2	-1	—	68	—	0.35	0.231
f011	91.934 (0.007)	10877.33 (0.85)	1.24	2	0	—	68	—	0.18	0.2266
f012 [†]	92.161 (0.010)	10850.59 (1.21)	1.89	2	1	38	68	0.07	0.00	—
f013	94.590 (0.032)	10571.94 (3.56)	0.38	1	—	37	—	0.02	—	—
f014	99.289 (0.004)	10071.59 (0.41)	0.22	2	0	—	63	—	-0.08	0.1221
f015*	99.411 (0.005)	10059.22 (0.47)	0.19	1	1	35	63	0.09	-0.16	0.1141

TABLE 2
 POSSIBLE COMBINATION FREQUENCIES (IN μHz) FOR $f_3 - f_2 - f_1 = \delta f$ WITH $\delta f < 0.0001$.
 AMPLITUDES (IN PPT) ARE PROVIDED IN COLUMNS 4 – 6.

f_1	f_2	f_3	A_1	A_2	A_3
76.174	135.710	211.884	0.16	0.35	3.30
99.411	118.866	218.277	0.19	1.31	1.14
105.632	193.670	299.302	2.92	0.22	0.42
158.845	774.149	932.994	1.51	0.22	0.62
253.194	312.699	565.893	1.21	0.13	0.21

TABLE 3
 LOG OF THE LOW-RESOLUTION SPECTROSCOPY OF KIC 3527751.

Mid-exposure date	Barycentric JD –2 455 000	S/N	RV km s^{-1}	RV _{err} km s^{-1}	Telescope	Observer
2010-07-28 01:32:16	405.5669179	107.4	6.9	3.1	WHT	RHØ
2010-07-28 05:02:45	405.7130811	82.7	-6.0	3.1	WHT	RHØ
2010-08-13 08:25:22	421.8535618	69.8	-1.2	6.1	KPNO	MDR/LHF
2010-08-13 08:36:39	421.8613996	65.3	-1.5	9.6	KPNO	MDR/LHF
2010-08-14 07:11:56	422.8025448	57.4	5.2	4.1	KPNO	MDR/LHF
2010-08-14 07:22:55	422.8101739	63.8	11.6	6.5	KPNO	MDR/LHF
2010-08-14 07:33:15	422.8173514	65.7	15.5	10.4	KPNO	MDR/LHF
2011-06-01 02:47:19	713.6181963	71.7	-13.0	6.1	NOT	JHT
2011-06-07 04:11:17	719.6767124	47.4	-5.1	6.3	NOT	JHT
2011-06-09 05:15:40	721.7214831	42.8	-15.3	6.3	NOT	JHT
2011-06-20 00:33:42	732.5259579	51.9	-11.0	5.1	NOT	JHT
2011-06-20 02:43:12	732.6158815	48.6	-5.8	5.9	NOT	JHT
2011-06-20 05:22:41	732.7266388	36.2	-5.9	5.7	NOT	JHT
2011-06-27 22:53:21	740.4564180	42.8	-35.0	8.5	NOT	JHT
2011-07-23 00:58:51	765.5437440	43.6	-26.9	9.8	NOT	JHT
2011-07-23 01:38:08	765.5710230	38.5	-29.0	11.2	NOT	JHT
2011-07-23 02:18:10	765.5988233	38.3	-13.4	7.5	NOT	JHT
2011-07-23 03:11:48	765.6360675	47.9	-37.7	9.8	NOT	JHT
2011-07-23 04:05:02	765.6730338	43.2	-34.8	11.2	NOT	JHT
2011-07-23 05:00:47	765.7117481	42.9	-33.0	13.4	NOT	JHT
2011-07-24 04:51:35	766.7053592	47.8	-17.0	9.7	NOT	JHT
2011-08-29 00:08:25	802.5080643	31.8	-76.3	10.4	NOT	JHT
2011-08-30 00:30:11	803.5231446	42.1	-24.7	10.4	NOT	JHT
2011-08-30 20:53:13	804.3724475	40.0	-23.2	10.9	NOT	JHT

termine effective temperature (T_{eff}), surface gravity ($\log g$), and photospheric helium abundance ($\log y = \log N_{\text{He}}/N_{\text{H}}$). The fitting procedure used was the same as that of Edelmann et al. (2003), using the metal-line blanketed LTE models of solar composition described in Heber et al. (1999). Mean values from these three fits were computed using the formal fitting errors as weights and systematics between observatories were then factored into the errors. The resultant measurements are indicated in Table 4 and we adopt the values of $T_{\text{eff}} = 27818 \pm 163$, $\log g = 5.35 \pm 0.03$, and $\log(N_{\text{He}}/N_{\text{H}}) = -2.99 \pm 0.04$.

3. Mode Identification

Prior to *Kepler*, observational mode identifications were extremely rare for sdB pulsators, leaving period matching between models and observations (the forward method) as virtually the only means of correlating periodicities to modes for sdB stars. However, using *Kepler* extended data sets, purely observational mode identifications using frequency multiplets and period spacings have become well-established techniques. We follow the examples of Baran et al. (2012) and Reed et al. (2011, 2014) in applying these methods to identify modes in KIC 3527751. To first order, stellar rotation removes azimuthal frequency degeneracy resulting in frequency multiplets appearing with $2\ell + 1$ members, with each member shifted by

$$\Delta\nu = \Delta m\Omega(1 - C_{n,\ell}) \quad (1)$$

from the $m = 0$ value (Ledoux 1951). Ω is the frequency of stellar rotation, and $C_{n,\ell}$ is the Ledoux constant which is nearly zero for p -modes and for g -modes depends on the mode degree as

$$C_{n,\ell} \approx \frac{1}{\ell(\ell + 1)}. \quad (2)$$

Similarly, g -modes may show radial overtones spaced evenly in *period* as

$$\Delta\Pi_\ell = \frac{\Pi_o}{\sqrt{\ell(\ell + 1)}} \quad (3)$$

where $\Delta\Pi_\ell = \Pi_{\ell,n+1} - \Pi_{\ell,n}$ and Π_o is the radial fundamental period. Even period spacings imply idealized homogenous stars using asymptotic relations ($n \gg \ell$). In practice, even period spacings have *not* been observed at short (where n is

not much greater than ℓ) or long (where frequency multiplets become spaced similar to period spacings) periods (Baran & Winans 2012; Østensen et al. 2014b; Reed et al. 2014).

3.1. Frequency Multiplets

g -mode multiplets: Uncovering multiplets in KIC 3527751 is extremely useful in associating periodicities with pulsation modes, ℓ and m . A cursory inspection of the most visible multiplets in the g -mode region reveals a common splitting near $0.23 \mu\text{Hz}$. Many of these multiplets have four or five peaks, meaning these are most likely $\ell = 2$ modes. (A discussion of how inclination affects the number of observed multiplet members is in §4.4) 22 multiplets with similar splittings were found and designated as $\ell = 2$ modes. In cases where the $m = 0$ component was ambiguous, we arbitrarily assigned it to the appropriate highest amplitude member. The average frequency splitting of the most easily distinguished $\ell = 2$ multiplets was $0.23 \pm 0.03 \mu\text{Hz}$. Triplets which displayed similar splittings were likewise designated as $\ell = 2$.

Though the overwhelming majority of multiplets were designated $\ell = 2$, some had splittings smaller than $0.23 \mu\text{Hz}$, often closer to $0.13 \mu\text{Hz}$. This value is the splitting we expect to see from Eqns. 1 and 2 for $\ell = 1$ multiplets. Nine multiplets had splittings near this value and were designated as $\ell = 1$. We find the average splitting of $\ell = 1$ multiplets to be $0.12 \pm 0.03 \mu\text{Hz}$. Altogether, we associated 123 frequencies with $\ell = 1$ and 2 modes using the frequency multiplet splitting method.

One multiplet present in KIC 3527751 ($f158 - f162$) at first glance appears to be a quintuplet, but the spacing between members is about double that expected for $\ell = 2$ multiplets. Additionally, there are two multiplets ($f164 - f169$ and $f190 - f197$) which contain too many members (six and eight) to be $\ell = 2$ modes and the splitting is slightly wider, consistent with the smaller Ledoux constant expected for $\ell = 4$ g -modes. In total, 19 frequencies are associated with these three multiplets, with an average $\Delta m = 1$ splitting of $0.27 \pm 0.04 \mu\text{Hz}$. We interpret these three multiplets to be $\ell = 4$ modes. Sample multiplets with their Lorentzian fits are shown in Fig. 3.

We note that $f159$ is at the known $1/\text{LC}$ space-

TABLE 4
SPECTROSCOPIC PARAMETERS FROM THE DETRENDED MEAN SPECTRA.

Telescope	T_{eff} [K]	$\log g$ [dex]	$\log (N_{\text{He}}/N_{\text{H}})$ [dex]
KPNO	27945 ± 133	5.35 ± 0.02	-2.97 ± 0.03
NOT1	27715 ± 102	5.32 ± 0.02	-3.01 ± 0.03
NOT2	27709 ± 102	5.33 ± 0.02	-3.02 ± 0.02
WHT	27913 ± 82	5.38 ± 0.01	-2.95 ± 0.03
Adopted	27818 ± 163	5.35 ± 0.03	-2.99 ± 0.04

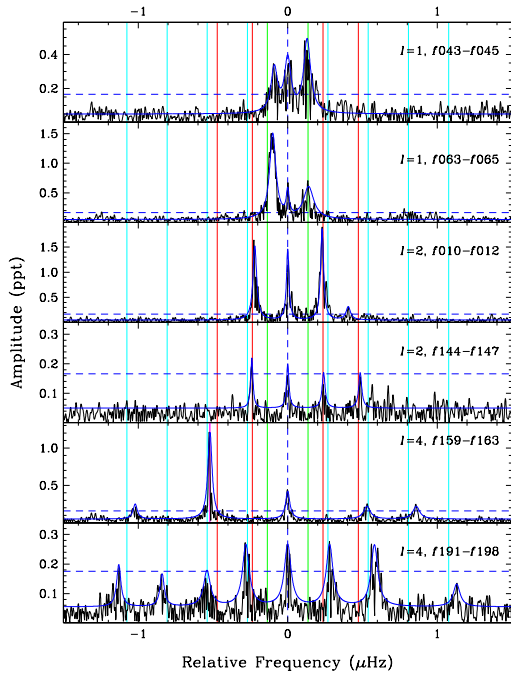


Fig. 3.— Sample frequency multiplets and Lorentzian fits for $\ell = 1, 2,$ and 4 modes. Frequency is relative to the center of the multiplet (dashed vertical blue line) with other vertical lines indicating the $\ell = 1$ (green), 2 (red), and 4 (cyan) multiplet spacings. The wide solid vertical (magenta) line indicates the $1/\text{LC}$ spacecraft artifact. The horizontal (blue) dashed line is the 5σ detection limit. Not all fitted frequencies have amplitudes that are significant in the full data set, but are during subsets.

craft artifact. Typically the $1/\text{LC}$ is *not* observed, but rather $8\text{-}10/\text{LC}$ more commonly are, yet this gave us pause. We examined the nearest star with SC data (KIC 3323887), processing those data in the same way as for KIC 3527751, to see if the $1/\text{LC}$ artifact appears. There was no signal at $1/\text{LC}$ in KIC 3323887. We also compared the sFT for f_{159} with other LC artifacts at 4531 ($8/\text{LC}$) and $5098 \mu\text{Hz}$ ($9/\text{LC}$), which show a harmonic frequency shift, since intrinsic frequencies become Doppler shifted due to the spacecraft’s orbit around the Sun after the heliocentric correction is applied. The sFT for f_{159} does not appear similar to those for $8/\text{LC}$ or $9/\text{LC}$ and so we suggest that f_{159} is intrinsic to KIC 3527751.

Another interesting multiplet includes $f_{213} - f_{225}$ which is shown in Fig. 4. Eight frequencies are spaced by 0.40 to $0.50 \mu\text{Hz}$ or 19 frequencies are spaced by 0.19 to $0.25 \mu\text{Hz}$ missing members corresponding to $m = \pm 3, 5,$ and 7 (with the $m = -1$ frequency listed as *tentative* in Table 1 since it is just below 5σ). If we assume the smaller spacing, then the average $\Delta m = 1$ frequency splitting would be $0.22 \pm 0.02 \mu\text{Hz}$ and the mode would be $\ell \geq 9$. However, the splittings would be slightly smaller than the $\ell = 2$ ones, which is contrary to Eqn. 2. On the other hand, if we assume the larger frequency splitting (with the outside pair just being chance alignments), then it would be an $\ell \geq 4$ multiplet, but with spacings of $0.45 \pm 0.03 \mu\text{Hz}$ which would be 67% larger than the other $\ell = 4$ multiplets. We tentatively assign it to the smaller splittings as an $\ell = 9$ multiplet in Table 1 with the caveat that low and variable amplitude signals are difficult to extract from the FT and may be imprecise.

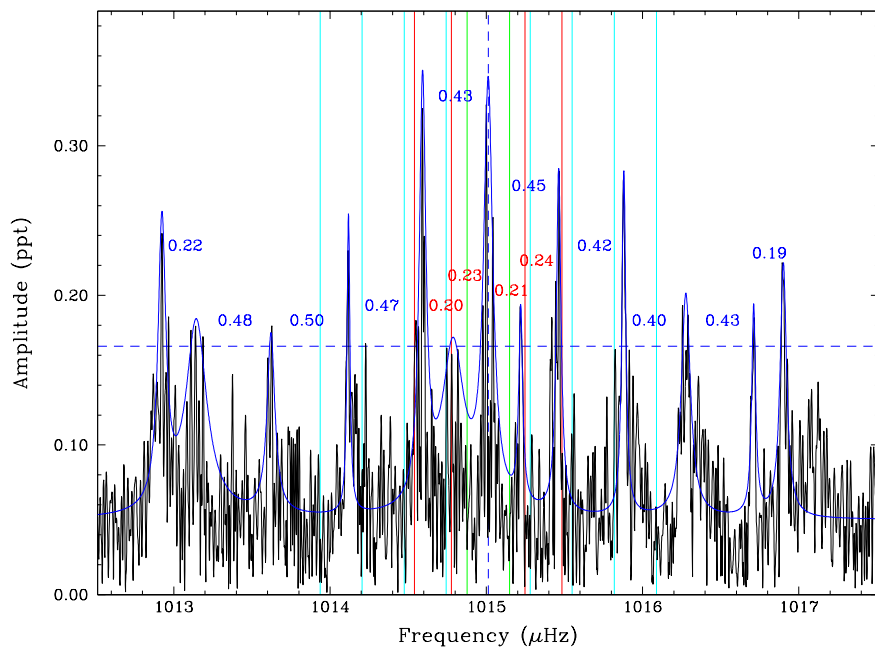


Fig. 4.— Possible high-degree multiplet. The solid black line is the FT from the entire data set with the blue lines the Lorentzian fits, as in Fig. 3 and the horizontal (blue) dashed line is the 5σ detection limit. The vertical lines indicate the central frequency (dashed) and the $\ell = 1$ (green), 2 (red), and 4 (cyan) multiplet spacings from Fig. 3. The numbers indicate the frequency spacings, in μHz .

***p*-mode multiplets:** Looking beyond about six minutes, where we expect *p*-mode pulsations to occur, there are 10 frequencies with amplitudes above the 5σ limit, not including known artifacts. These fall into sets near 2780 and 3700 μHz . Additionally, the set near 2780 μHz has four frequencies with amplitudes above the 4σ limit which perfectly fit into two sets of frequency multiplets (f_{239} – f_{241} and f_{244} – f_{245}).

These 14 frequencies bear some resemblance to Balloon090100001 (Baran et al. 2009). The highest-amplitude frequency (f_{238}) occurs roughly where the radial fundamental is typically found in such stars, followed by a much lower amplitude triplet (f_{239} - f_{241}) and quintuplet (t_{242} - f_{246}), in order of ascending frequency. These multiplets have consistent frequency splittings of 0.7 to 0.8 μHz . Beyond this group is another group near 3700 μHz with inconsistent frequency splittings, also similar to what is observed for Balloon090100001. The ratio of the f_{238} – f_{246} group near 2800 μHz to the f_{247} – f_{251} group near 3700 μHz is 0.76 which is similar to, but slightly larger than, the value of 0.7 calculated for Balloon090100001 (Baran et al. 2009).

Based on the consistent frequency splittings and pattern similarities with Balloon090100001, we assign the first nine *p*-mode frequencies as an $\ell = 0$ singlet, an $\ell = 1$ triplet and an $\ell = 2$ quintuplet. The remaining five frequencies are most likely the next overtone sequence, but we cannot assign specific modes to frequencies as their splittings are inconsistent.

3.2. Period spacings

To begin the hunt for period spacing sequences in KIC 3527751, we applied a Kolmogorov-Smirnov (KS) test, using the periods listed in Table 1. However, all 251 periods do not produce any distinguishing peaks. Since geometric cancellation increases with increasing ℓ (Pesnell 1985), we did a KS test on just the 100 highest-amplitude periods. This produced a substantial peak at 265 seconds with a lesser one at 153 seconds, right where expected from Eqn. 3 ($265/\sqrt{3} = 153$ seconds). Both KS tests are shown in the top panels of Fig. 5.

Next we produced Echelle diagrams using the spacings indicated by the KS test. These are shown in Fig. 6 with different symbols indicat-

ing mode identifications. Even with these tools, we imposed additional conditions on our search for period sequences. We began by examining i) the high-amplitude periodicities under the assumption that they are $\ell = 1$ (as indicated by the strong peak in the KS test) and ii) using the multiplets (both $\ell = 1$ and 2) as starting points for sequences. We could easily identify a sequence for both $\ell = 1$ and 2 modes. We detected 35 $\ell = 1$ periodicities and 95 $\ell = 2$ periodicities that follow sequences within a small margin. We assigned radial indices (n) to the members of these sequences, estimating that the radial fundamental mode would appear near 600 seconds; a rough estimate for stars with $\log g \approx 5.2$. This resulted in period spacings of 266.4 ± 0.2 and 153.2 ± 0.2 seconds for $\ell = 1$ and 2, respectively, in good agreement with the survey results of Reed et al. (2010).

Our best-estimate mode identifications, using multiplets and period spacings, are provided in Columns 5 through 8 of Table 1.

4. Discussion

Now that mode identifications have been established, they can be examined using the tools applied in our previous papers.

4.1. Unidentified Periodicities

Ideally, every periodicity detected in KIC 3527751 would be associated with a mode or a combination frequency. With some degree of certainty, we have identified three $\ell = 4$ multiplets, and possibly even an $\ell = 9$ multiplet, which invites a search for more high-degree periodicities. To do this, we prewhiten the KS test. We remove our assigned $\ell = 1$ modes, $\ell = 2$ modes, and then both. Of the 79 periodicities longer than 800 s not identified as $\ell = 1$ or 2, 19 are identified as $\ell = 4$ and 13 as part of a possible $\ell = 9$ multiplet, leaving just 45 of 225 *g*-mode periodicities ($f < 1100 \mu\text{Hz}$) as unidentified. The bottom panels of Fig. 5 show the period prewhitening sequences. When the $\ell = 2$ sequence is removed, a second peak appears shortward of the $\ell = 1$ peak, which could indicate deviations or multiplet structure in that sequence. However, when both $\ell = 1$ and 2 are removed, some of that peak remains, indicating that we may not be catching all

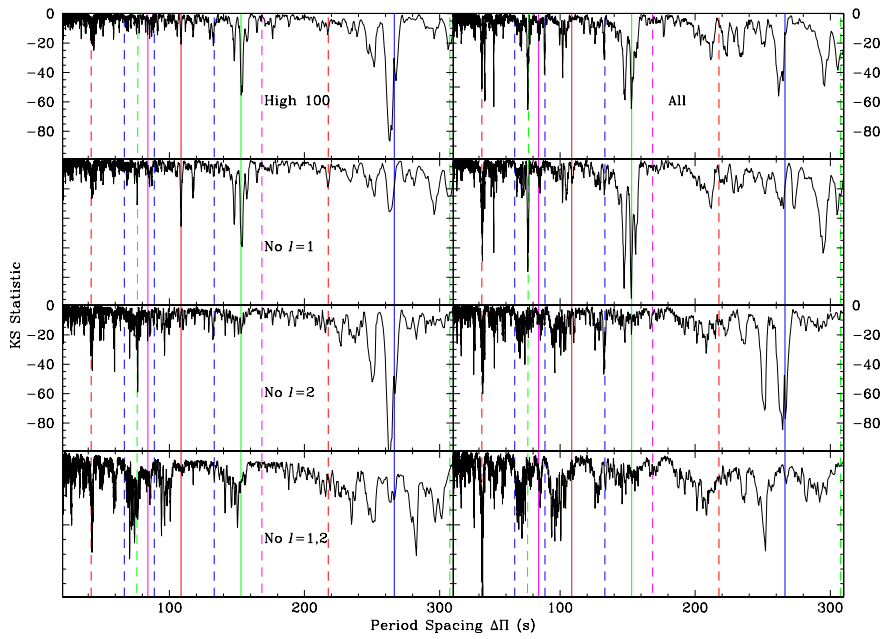


Fig. 5.— KS diagram indicating period spacing sequences. The left panels only include the highest 100 amplitude periods while the right panels include all periods longer than 900 seconds. Solid lines near 153 and 266 seconds indicate the $\ell = 2$ and 1 sequences, respectively, and the solid lines near 84 and 109 seconds indicate where the $\ell = 4$ and 3 sequences should appear. Dashed lines indicate sequence aliases. (Color-coded version appears on-line.)

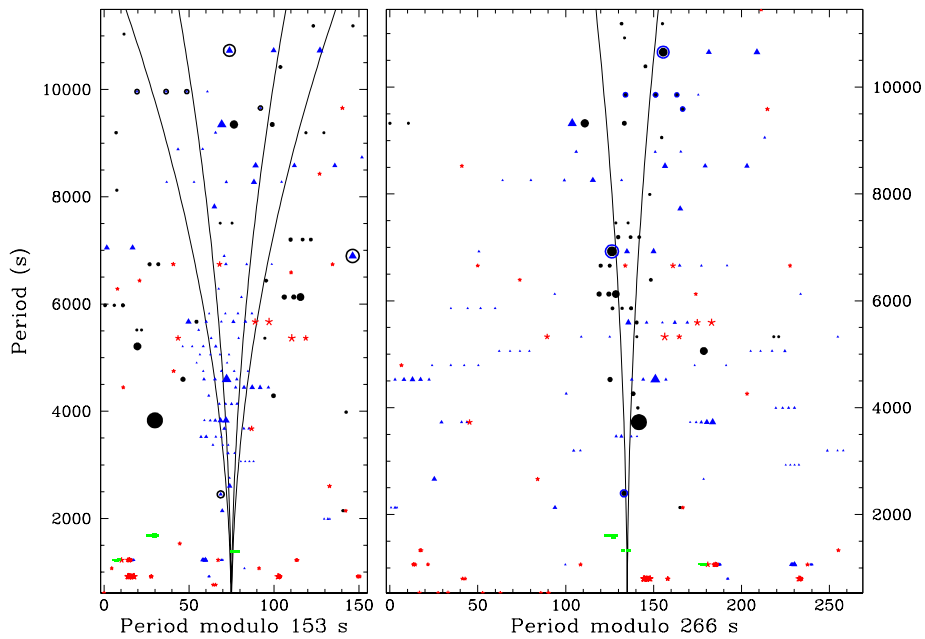


Fig. 6.— Echelle diagrams for $\ell = 1$ (right) and 2 (left) modes. Black circles indicate our identified $\ell = 1$ modes, blue triangles $\ell = 2$ modes, green squares $\ell = 4$ and 9 modes, and red stars indicate periods which are not associated with a mode. Periods which could be either $\ell = 1$ or 2 are indicated with an extra colored circle (black in the left panel and blue in the right panel). Point sizes are (logarithmically) scaled with amplitude and vertical lines indicate the extent of frequency multiplet splittings.

of the $\ell = 1$ sequence. However, no new peaks appear where we would expect the higher-degree sequences to be (indicated by vertical lines near 109 and 84 seconds for the $\ell = 3$ and 4 sequences, respectively). The three $\ell = 4$ multiplets we detect have spacings between them of 257 (3×86) and 223 (3×74) seconds which are close to $3 \times$ the expected value. Yet we have to conclude that the KS plots do not reveal obvious peaks where $\ell = 3$ or 4 modes should be. Since many of the unidentified periods are short (53 of these have periods below 1800s), they could well be $\ell = 1$ and 2 modes which do not fit the period sequences because they are low radial (n) order.

4.2. Trapped Modes

Structural models have indicated significant mode trapping in the He–H transition zone of sdB stars (Miller Bertolami et al. 2012; Hu et al. 2009; Charpinet et al. 2002). Period spacing sequences argued against significant mode trapping (see the discussion in §3 of Reed et al. 2011) until the recent discovery of trapped modes in the sdBV star KIC 10553698A (Østensen et al. 2014b). Thus it is prudent to search for trapped modes in each sdBV star analyzed. Unfortunately, not finding trapped modes is like not finding a binary star— one can have positive detections, but it is nearly impossible to conclusively rule them out. For KIC 3527751, there are four periodicities (f_{023} , f_{024} , f_{084} , and f_{085}) with $\ell = 1$ -like multiplet splittings which do not fit into the period sequence. These can be seen in the Echelle diagram (Fig 6), but are most easily seen in a reduced period plot (Figure 7), such as that in Østensen et al. (2014b). Reduced period plots are also commonly shown in modeling papers, such as those previously referenced. Periods are converted to degree-independent reduced periods by multiplying by $\sqrt{\ell(\ell + 1)}$, which also makes the period spacings degree independent. The trapped $\ell = 1$ modes deviate shortward from the main spacing near 380 seconds.

However, there are no corresponding trapped $\ell = 2$ modes. In regular period, the positions where the trapped $\ell = 2$ modes would occur are near 3270 and 5430 seconds. There are no available periodicities near 3270 seconds ($306 \mu\text{Hz}$) even when looking below the 4σ limit. So there are *no* candidates for a trapped $\ell = 2$ mode corresponding to this trapped $\ell = 1$ mode. For the

second trapped mode, there is a single peak at 5457 seconds that we assign as a trapped $\ell = 2$ mode corresponding to the trapped $\ell = 1$ mode near a reduced period of 13000, but mark it in Fig. 7 with an open symbol.

Since the sequences were not complete, we also looked for periodicities of missing overtones, to complete the sequences. A few more possible periods were detected with amplitudes between 4 and 5σ , and are marked with open symbols, and we also detected some which overlap the other sequence. Equation 3 predicts that sequences overlap, so mode degeneracy is expected. We have marked those periods with crosses and note that these mode identifications are not favored because of multiplet splittings.

The $\ell = 2$ sequence extends well beyond the $\ell = 1$ sequence and there are some indications of trapped modes at either end. Of course at the short end, the radial orders are small, where asymptotic behavior is not expected anyway and at the longer end, there are many missing radial orders, so a lot of ambiguity exists. We include them for completeness.

This would be the second sdBV star to show strong indications of trapped modes, contrary to what was indicated in Reed et al. (2011).

4.3. Radially Differential Rotation

Previous papers (e.g. Baran et al. 2012) have used multiplets to determine stellar rotation periods and since many multiplets were detected in KIC 3527751, we do it here too. We separate the pulsations into p - and g -modes and further separate the g -modes by degree, ℓ . We do this because the splitting in g -modes is degree-dependent whereas p -modes have small Ledoux constants (e.g. Van Grootel et al. 2008). For the g -modes, we calculated the stellar rotation period to be 46 ± 8 , 41 ± 5 , and 40 ± 5 days for the $\ell = 1, 2$, and 4 multiplets, respectively. These are all in close agreement. For the p -modes, using a Ledoux constant of zero, we calculated a stellar rotation period of 15.3 ± 0.7 days. We note that while several members of the two p -mode multiplets have low amplitudes, the frequency splittings are remarkably uniform with comparatively large splittings of $0.74 \mu\text{Hz}$. These are shown in the bottom two panels of Fig. 8 with two g -mode multi-

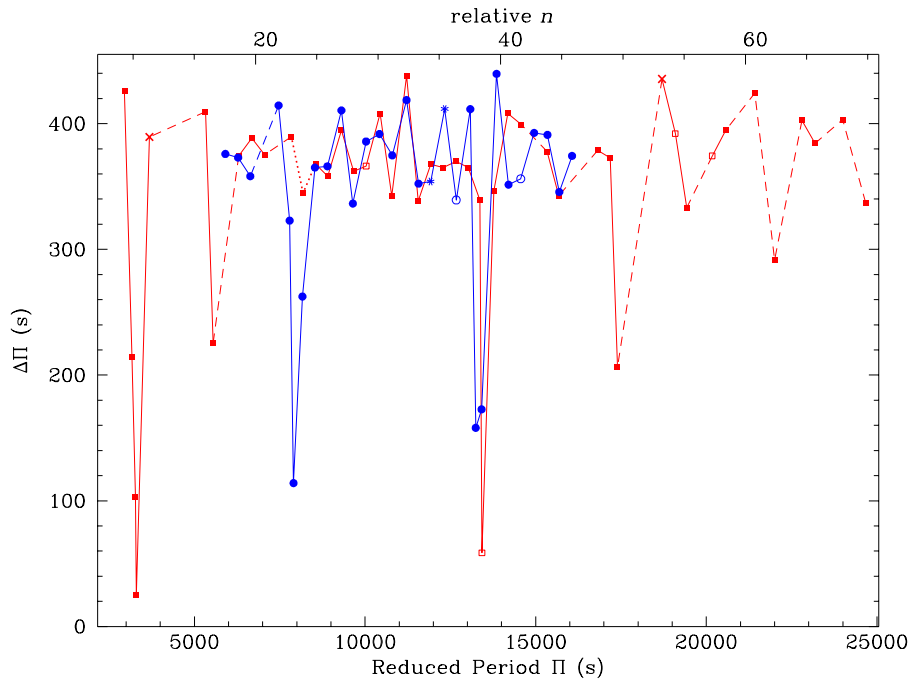
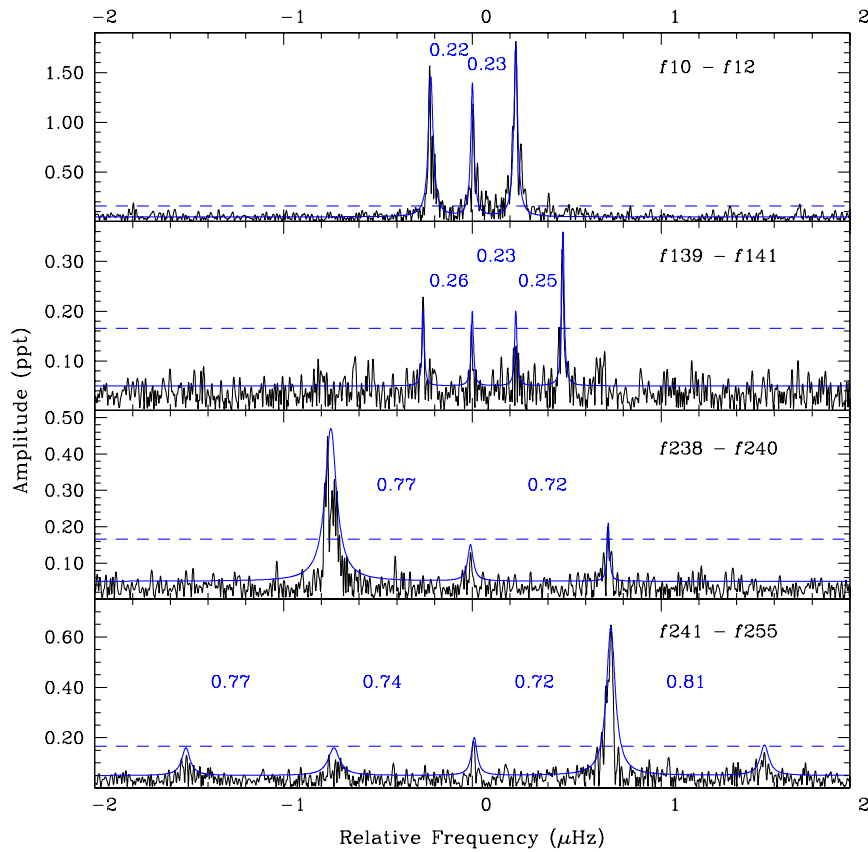


Fig. 7.— Reduced periods, $\Pi = P\sqrt{\ell(\ell + 1)}$, indicating trapped modes. Circles (blue) indicate the $\ell = 1$ sequence and squares (red) indicate the $\ell = 2$ sequence. Open symbols indicate periodicities discovered as the result of a search for missing overtones and trapped $\ell = 2$ modes, as discussed in the text, and crosses indicate modes with the same period as that of a different mode (e.g. an $\ell = 1$ mode previously identified as $\ell = 2$). Dashed lines indicate missing overtones and dotted lines in the $\ell = 2$ sequence indicate that a trapped mode is missing.



[t]

Fig. 8.— Frequency multiplets indicating radially differential rotation. The top two panels show g -mode multiplets and the bottom two panels p -mode multiplets. Numbers indicate the spacings between frequencies.

plets in the top panels.

Here we arrive at a contradiction; the two p -mode multiplets indicate a spin period of 15.3 ± 0.7 days while the g -mode multiplets indicate a period near 43 days. We can imagine three possibilities which would generate these results; i) the intrinsic p -mode multiplets are actually spaced at $1/3$ our observed value, ii) KIC 3527751 is a pair of sdBV stars with one a p -mode pulsator rotating with a period near 15 days and the other a g -mode pulsator rotating with a period near 43 days, or iii) KIC 3527751 is differentially rotating. We discuss all three possibilities below, but as to not leave the reader in too much suspense, we discount options i and ii and highly favor option iii.

For option i to be correct, the $f_{239} - f_{241}$ triplet would need to be $\ell, m = 3, -3; 3, 0; \text{ and } 3, +3$ and the $f_{242} - f_{246}$ quintuplet would need to be $\ell, m = 6, -6; 6, -3; 6, 0; 6, +3; \text{ and } 6, +6$. This seems quite unlikely since both of these have quite high geometric cancellation factors (Pesnell 1985). In addition, there is no pulsation inclination where the $m = 1, 2, 4, \text{ and } 5$ modes have a common node. Yet we cannot summarily rule this out as we seem to detect $\ell = 4$ and possibly 9 modes in the g -mode regime. However, in the g -mode cases, there are many more higher-amplitude periodicities whereas in the p -mode range there would only be one. As such, we would have to question why the $\ell = 0, 1, \text{ and } 2$ modes are not excited to observable levels when their cancellation factors are so much smaller. Additionally, the frequency/amplitude pattern is similar to what has been observed in the sdBV star Balloon 090100001 (as discussed in §3.1), making option i unlikely.

Option ii seems unlikely from the outset as an sdB+sdB binary has never been observed, and only about 80% of cool sdB stars pulsate with g -modes and 10% of hotter sdB stars pulsate with p -modes. We could rule out this possibility immediately if members of p - and g -mode pulsations were in combination frequencies. Unfortunately, that is not the case as our possible combination frequencies are g -mode (or mixed character) periodicities only (Table 2). Several other sdB stars have been discovered to be binary via their *Kepler* lightcurves which show signs of Doppler beaming, tidal distortions, and/or eclipses (e.g. Telting et al. 2012; Bloemen et al. 2012). These effects

should only occur for relatively short-period binaries, and so we re-processed KIC 3527751’s data prior to long-term trend removal and this time detrended, month-by-month, only for periods longer than eight or ten days. This detrending leaves three, closely-spaced, low-amplitude peaks in the FT at 3.933, 3.962, and 4.026 μHz (2.94, 2.92, and 2.87 days, respectively) with amplitudes of 0.051, 0.042, and 0.056 ppt, respectively. Already, with three peaks, these are highly unlikely to be signatures of binarity, but are most likely spurious noise which was not properly removed. But to complete this exercise, using the Doppler beaming procedure of Telting et al. (2012, specifically equation 2), we calculate a velocity amplitude of the binary’s orbital motion of $23.6 \text{ km}\cdot\text{s}^{-1}$ from the flux amplitudes. From our 23 RV measurements, we determine an RV amplitude of $16.5 \pm 3.2 \text{ km}\cdot\text{s}^{-1}$ for this period. These velocities are not consistent with each other, and assuming sdB stars of canonical mass ($0.48 M_{\odot}$) would require inclinations below 15° . This combination of evidence makes it extremely unlikely that KIC 3527751 is a binary pair of pulsating sdB stars.

Therefore it is far more likely that KIC 3527751 is differentially rotating (option iii) and we consider this to be the case. p -mode pulsations only sample the envelope whereas g -mode pulsations penetrate the He core and so are sensitive to conditions deeper within the star (see example propagation diagrams in Charpinet et al. 2014). As such, the g -mode-derived rotation rate is sensing deep into the star and the p -mode rate is sensing the outer regions. There is overlap in the propagation diagram of Charpinet et al. (2014), so the core rate is likely slower than indicated by the g modes, but these results conclude that the core is rotating at least three times slower than the envelope. To determine a more precise value would require appropriate models constructed using the observational constraints (mode IDs, period spacing/trapping sequences, etc.) of this paper to calculate the proper propagation diagram. To date, no detailed models have been published which fully incorporate the detailed seismic constraints provided from Kepler data. Interestingly, a similar discovery has been detected in *Kepler* observations of a pulsating main sequence A star (Kurtz et al. 2014), although in that case, the core is only rotating about 5% slower than the enve-

lope. Radially differential rotation has also been measured in red horizontal branch stars, though in that case the core is rotating faster than the envelope (Beck et al. 2012).

4.4. Pulsation Inclination Angle

As shown in Charpinet et al. (2011a); Reed et al. (2005); Pesnell (1985), geometric cancellation is inclination and m -dependent, which means we can determine the inclination angle of the pulsation axis to our line-of-sight using multiplet amplitudes. For observations which span several amplitude e-folding timescales, it is reasonable to presume that all amplitudes of all multiplet members have reached average amplitudes and then their relative heights indicate the inclination angle. However, as Fig. 2 indicates, for KIC 3527751 it does not appear that the data span more than a single amplitude variation cycle, and so this assumption is likely not valid. Yet we can place constraints using surface nodes, where geometric cancellation is complete, to omit inclination ranges. The $\ell = 1$ multiplet amplitudes, while inconsistent between multiplets, have roughly equal amplitudes for all members, indicative of intermediate inclinations ($30 - 60^\circ$). Several of the $\ell = 2$ multiplets are quadruplets, a few are full quintuplets, and some are only triplets. Since all members are present in various multiplets, it indicates inclinations above 15° (which would not have $m \neq 0$ components) and below 75° (which would suppress $m = 2$ components). Additionally, there is an $m = 0$ node line at $i = 54^\circ$ which eliminates inclinations between 50 and 65° . The $\ell = 4$ multiplets are more sensitive to the inclination angle, yet are inconsistent between multiplets. The $566 \mu\text{Hz}$ multiplet has only even m members while the other two have roughly-equal amplitudes for all members. As such, we have to presume that no members are suppressed. Since $\ell = 4$ node lines appear at $i = 0, 32, 48, 67, 70,$ and 90° , inclinations within a few degrees would be suppressed. What is left are inclinations between 35 and 45° , based solely on multiplet members being visible.

4.5. Pulsation Density

We can also examine where the pulsations seem to be most easily driven. Near instability boundaries, it would be expected that fewer periodic-

ities would be driven and so mapping pulsation density with overtone may provide constraints on the driving region itself (as in Fig. 9 of Jeffery & Saio 2006). We use multiplet members as a proxy of driving power; the more multiplet members observed, the more driving power we presume that mode to have. There are methods for doing this involving pulsation amplitudes (e.g. Mukadam et al. 2006), however considering the variability observed over the duration of the observations, this seems a difficult proposition- Should we calculate the total power when the amplitudes are maximum or median? Should we consider multiple times per multiplet when each member is maximum, or choose only one time when most members are visible? The scheme we decided to use, number of multiplet members, is simpler in two ways: it is binary- either multiplet members are detected or they are not, and it imposes no time or amplitude constraints. The members do not have to be simultaneously detected. Once structure and pulsation models are sufficiently mature to accurately reflect the observed pulsation behavior, our scheme may prove not to be the best. However, with the information currently in hand, it seems more robust than using amplitudes and a good beginning point for determining pulsation instability.

Figure 9 shows multiplet members by radial order with the densest region between $n = 20$ and 40 for $\ell = 1$ and 2 while the $\ell = 4$ multiplets have $15 \leq n \leq 20$. It is interesting that the $\ell = 4$ modes have lower orders as they should be very sensitive to pulsation power to drive them to observable amplitudes. Yet as we are not producing models, we only indicate their relative regions as another constraint for those who do. Once all the *Kepler*-observed sdBV stars are analyzed, a comparison between different pulsators should map the instability region.

5. Summary and Conclusions

We have detected 251 periodicities in KIC 3527751 using 38 months of virtually continuous *Kepler* data. Most of these are in the g -mode regime of long periods, 14 should be p -modes with periodicities shorter than six minutes, and 38 periods are between 9 and 20 minutes and could be modes of mixed character. We recovered all but one of

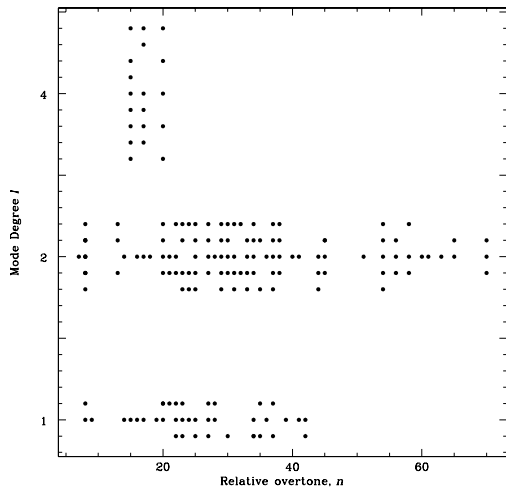


Fig. 9.— Periodicities arranged by degree and radial index used to indicate where maximum driving occurs.

the periodicities detected by Reed et al. (2010), including those in the p -mode regime. We do see two peaks near the missing frequency, at $544 \mu\text{Hz}$ in Reed et al. (2010), but since they are both slightly below our 5σ limit, we did not list them.

Similar to most other *Kepler*-observed sdBV stars, amplitudes and sometimes frequency/phase variations occur throughout the extended dataset, making traditional frequency-fitting and prewhitening tools unfeasible. We therefore used sFTs and Lorentzian fitting to attempt to disentangle the frequency content. Even so, there are regions which are extremely messy, with amplitude variations and frequency variations which make modes seemingly cross each other. For these regions, extractions are somewhat subjective as portions of FTs are chosen from the sFT for which the pulsations are most clearly seen. This usually means the frequencies are at their most separated which could apply a bias to the results. We encourage others to examine the accompanying figures of sFTs, or even better develop their own methods, for determining frequencies and amplitudes, and their variations.

In an attempt to understand the pulsations, we applied a wide variety of tools which have previously been used. Some of these did not reveal new relationships: prewhitening the KS test did not show any peaks indicative of $\ell \geq 3$ modes and the density of mode multiplets (Fig. 9) are not consistent between degrees. All three of the mode identification methods did work well, resulting in 75% of the periodicities having assigned modes.

Our multiplet analysis also revealed three $\ell = 4$ multiplets and possibly an $\ell = 9$ multiplet. Several other *Kepler*-observed sdB pulsators also have high-degree ($\ell \geq 3$) modes, including KIC 7668647 which has an $\ell = 8$ multiplet (Teltting et al. 2014). High-degree modes have long been a staple of sdB asteroseismology to explain the density of periodicities of p -mode pulsations (see the discussion of Reed et al. 2007, §5.3 and Fig. 15). The precision and duration of *Kepler* data allowed us to detect periodicities with amplitudes $1/45$ of the highest one. With this large dynamic range, we *should* be seeing high-degree modes, yet only with confirming multiplet structure can we be certain. As such, even *Kepler*-observed sdB pulsators have a large number of unidentified periodicities which could be

high-degree modes, but there is no way to be certain.

Since the Ledoux constant is degree-dependent for g -modes, the rotation period ($1/\Omega$) determined from different degrees can be used to check if the multiplet splittings agree with predictions from Eqns. 1 and 2. As stated in §4.3, the rotation periods from the $\ell = 1, 2$, and 4 modes are calculated to be 46 ± 8 , 41 ± 5 , and 40 ± 5 days, respectively. Since these periods all agree, the mode-dependent Ledoux constants fit those predicted from Eqn 2, supporting our mode identifications.

Remarkable features in KIC 3527751 include mode trapping and radially differential rotation. The case for mode trapping is less sure than that of Østensen et al. (2014b), where long complete sequences of overtones were found. In our case, there are several missing and so we have had to average across those missing overtones. While we have two nice $\ell = 1$ trapped regions, with mode identifications based on multiplet splittings, we do not detect one of the corresponding $\ell = 2$ trapped modes and the other occurs where a non-trapped $\ell = 1$ mode is, making its identification uncertain. So we have good examples of $\ell = 1$ trapped modes, but not for $\ell = 2$.

We detect g -mode multiplet splittings for three degrees ℓ which provide the same rotation period which is substantially different from that derived from two p -mode multiplets. We examined the prospect that KIC 3527751 could actually be a binary set of pulsating stars, and while we cannot completely rule it out, it is exceedingly unlikely, as is the possibility that the p -mode multiplets are really spaced like the g -mode ones, but are just missing members. Therefore, we suggest that KIC 3527751 is differentially rotating in the radial direction with the core rotating nearly three times more slowly. This is opposite to that described by Kawaler & Hostler (2005), who predicted rapidly rotating cores via conservation of angular momentum in a contracting core. This could be a clue to the mass loss mechanism itself and a bit of a dichotomy. Either the core must preferentially spin down during mass loss, or the entire star must spin down with the envelope subsequently being spun-up. The differential rotation of KIC 3527751 allows various mechanisms to be tested.

Funding for this research was provided by the

National Science Foundation grants #1009436 and #1312869. Any opinions, findings, and conclusions or recommendations expressed in this material are those of the author(s) and do not necessarily reflect the views of the National Science Foundation. HF was supported by the Missouri Space Grant Consortium, funded by NASA. This work was partially supported by Polish National Science Center under project No. UMO-2011/03/D/ST9/01914.

This paper includes data collected by the *Kepler* mission. Funding for the *Kepler* mission is provided by the NASA Science Mission directorate. Some/all of the data presented in this paper were obtained from the Mikulski Archive for Space Telescopes (MAST). STScI is operated by the Association of Universities for Research in Astronomy, Inc., under NASA contract NAS5-26555. Support for MAST for non-HST data is provided by the NASA Office of Space Science via grant NNX13AC07G and by other grants and contracts.

The spectroscopic observations used in this work were obtained with the Mayall Telescope of Kitt Peak National Observatory, which is operated by the Association of Universities for Research in Astronomy under cooperative agreement with the National Science Foundation; the William Herschel Telescope located at the Observatorio del Roque de los Muchachos (ORM) and operated by the Isaac Newton Group; and the Nordic Optical Telescope also at the ORM and operated jointly by Denmark, Finland, Iceland, Norway, and Sweden.

We thank the Referee for suggestions which improved the paper.

REFERENCES

- Baran, A., Oreiro, R., Pigulski, A., et al. 2009, MNRAS, 392, 1092
- Baran, A. S., & Winans, A. 2012, Acta Astron., 62, 343
- Baran, A. S., Reed, M. D., Stello, D., et al. 2012, MNRAS, 424, 2686
- Beck, P. G., Montalbán, J., Kallinger, T., et al. 2012, Nature, 481, 55
- Bloemen, S., Marsh, T. R., Degroote, P., et al. 2012, MNRAS, 422, 2600

- Charpinet, S., Brassard, P., Van Grootel, V., & Fontaine, G. 2014, in *Astronomical Society of the Pacific Conference Series*, Vol. 481, 6th Meeting on Hot Subdwarf Stars and Related Objects, ed. V. van Grootel, E. Green, G. Fontaine, & S. Charpinet, 179
- Charpinet, S., Fontaine, G., Brassard, P., & Dorman, B. 2002, *ApJS*, 139, 487
- Charpinet, S., Fontaine, G., Brassard, P., et al. 2011a, *Nature*, 480, 496
- Charpinet, S., Van Grootel, V., Fontaine, G., et al. 2011b, *A&A*, 530, A3
- Conroy, K. E., Prša, A., Stassun, K. G., et al. 2014, *AJ*, 147, 45
- Edelmann, H., Heber, U., Hagen, H.-J., et al. 2003, *A&A*, 400, 939
- Heber, U. 2009, *ARA&A*, 47, 211
- Heber, U., Reid, I. N., & Werner, K. 1999, *A&A*, 348, L25
- Hu, H., Nelemans, G., Aerts, C., & Dupret, M. 2009, *A&A*, 508, 869
- Jeffery, C. S., & Saio, H. 2006, *MNRAS*, 371, 659
- Kawaler, S. D., & Hostler, S. R. 2005, *ApJ*, 621, 432
- Kurtz, D. W., Saio, H., Takata, M., et al. 2014, *MNRAS*, 444, 102
- Ledoux, P. 1951, *ApJ*, 114, 373
- Miller Bertolami, M. M., Córscico, A. H., & Althaus, L. G. 2012, in *Astronomical Society of the Pacific Conference Series*, Vol. 452, Fifth Meeting on Hot Subdwarf Stars and Related Objects, ed. D. Kilkenny, C. S. Jeffery, & C. Koen, 175
- Mukadam, A. S., Montgomery, M. H., Winget, D. E., Kepler, S. O., & Clemens, J. C. 2006, *ApJ*, 640, 956
- Østensen, R. H. 2010, *Astronomische Nachrichten*, 331, 1026
- Østensen, R. H., Reed, M. D., Baran, A. S., & Telting, J. H. 2014a, *A&A*, 564, L14
- Østensen, R. H., Telting, J. H., Reed, M. D., et al. 2014b, *A&A*, 569, A15
- Østensen, R. H., Green, E. M., Bloemen, S., et al. 2010a, *MNRAS*, 408, L51
- Østensen, R. H., Silvotti, R., Charpinet, S., et al. 2010b, *MNRAS*, 409, 1470
- Østensen, R. H., Degroote, P., Telting, J. H., et al. 2012, *ApJ*, 753, L17
- Pablo, H., Kawaler, S. D., & Green, E. M. 2011, *ApJ*, 740, L47
- Pablo, H., Kawaler, S. D., Reed, M. D., et al. 2012, *MNRAS*, 422, 1343
- Pesnell, W. D. 1985, *ApJ*, 292, 238
- Reed, M. D., Brondel, B. J., & Kawaler, S. D. 2005, *ApJ*, 634, 602
- Reed, M. D., Foster, H., Telting, J. H., et al. 2014, *MNRAS*, 440, 3809
- Reed, M. D., Terndrup, D. M., Zhou, A.-Y., et al. 2007, *MNRAS*, 378, 1049
- Reed, M. D., Kawaler, S. D., Østensen, R. H., et al. 2010, *MNRAS*, 409, 1496
- Reed, M. D., Baran, A. S., Quint, A. C., et al. 2011, *MNRAS*, 414, 2885
- Telting, J. H., Østensen, R. H., Baran, A. S., et al. 2012, *A&A*, 544, A1
- Telting, J. H., Baran, A. S., Nemeth, P., et al. 2014, *A&A*, 570, A129
- Tenenbaum, P., Jenkins, J. M., Seader, S., et al. 2014, *ApJS*, 211, 6
- Van Grootel, V., Charpinet, S., Fontaine, G., & Brassard, P. 2008, *A&A*, 483, 875
- Van Grootel, V., Charpinet, S., Fontaine, G., et al. 2010, *ApJ*, 718, L97

This 2-column preprint was prepared with the AAS L^AT_EX macros v5.2.

TABLE 1

TABLE OF ASTEROSEISMIC QUANTITIES. COLUMN 1 PROVIDES A LABEL FOR THE PERIODICITY, COLUMNS 2 AND 3 THE FREQUENCY AND PERIOD, WITH ERRORS IN PARENTHESES, AND COLUMN 4 THE OBSERVED AMPLITUDE. COLUMNS 5 THROUGH 8 PROVIDE OUR BEST ESTIMATE MODE IDENTIFICATIONS, COLUMNS 9 AND 10 PERIOD SPACING DEVIATIONS, AND COLUMN 11 THE FREQUENCY SPLITTING (FROM THE SUBSEQUENT FREQUENCY) OF MULTIPLLET MEMBERS. [†] INDICATES PERIODICITIES DETECTED BY REED ET AL. (2010) AND * INDICATES FREQUENCIES WHICH ARE LISTED IN TABLE 2 AS PART OF A COMBINATION FREQUENCY. PERIODICITIES LISTED WITH “T”’S INSTEAD OF “F”’S IN THE ID COLUMN ARE BELOW THE 5 σ LIMIT AND THEREFORE CONSIDERED *tentative*.

ID	Freq. μHz	Period sec.	Amp. ppt	ℓ ...	m ...	$n_{\ell=1}$...	$n_{\ell=2}$...	$(\frac{\Delta P}{P})_{\ell=1}$...	$(\frac{\Delta P}{P})_{\ell=2}$...	δf μHz
f001	72.026 (0.015)	13883.84 (2.91)	0.17							
f002*	76.174 (0.010)	13127.84 (1.68)	0.16							
f003	77.630 (0.024)	12881.62 (3.99)	0.40							
f004	84.314 (0.006)	11860.43 (0.86)	0.16							
f005	84.790 (0.006)	11793.84 (0.81)	0.17							
f006	85.428 (0.016)	11705.79 (2.16)	0.24							
f007	87.851 (0.008)	11382.91 (1.04)	0.24	1	-1	40		0.06		0.1809
f008	88.032 (0.010)	11359.52 (1.31)	0.32	1	0	40		-0.02		
f009	90.130 (0.019)	11095.08 (2.34)	0.20	1		39		-0.02		
f010	91.703 (0.008)	10904.73 (0.91)	1.64	2	-1		68		0.35	0.231
f011	91.934 (0.007)	10877.33 (0.85)	1.24	2	0		68		0.18	0.2266
f012 [†]	92.161 (0.010)	10850.59 (1.21)	1.89	2	1	38	68	0.07	0.00	
f013	94.590 (0.032)	10571.94 (3.56)	0.38	1		37		0.02		
f014	99.289 (0.004)	10071.59 (0.41)	0.22	2	0		63		-0.08	0.1221
f015*	99.411 (0.005)	10059.22 (0.47)	0.19	1	1	35	63	0.09	-0.16	0.1141
f016	99.525 (0.007)	10047.69 (0.69)	0.23	2	1		63		-0.24	0.176
f017	99.701 (0.012)	10029.95 (1.18)	0.22	1	-1	35	63	-0.02	-0.35	
f018	101.589 (0.020)	9843.59 (1.94)	0.26							
f019	102.083 (0.006)	9795.95 (0.61)	0.21	1 or 2		34	61	0.11	0.12	
f020	105.304 (0.014)	9496.32 (1.22)	0.63	1	-1	33		-0.02		0.248
f021 [†]	105.552 (0.019)	9474.00 (1.68)	1.71	1	1	33		-0.10		0.08
f022*	105.632 (0.012)	9466.83 (1.08)	2.92	2	0		59		-0.03	
f023	106.678 (0.008)	9374.00 (0.70)	0.20	1	-1					0.128
f024	106.806 (0.019)	9362.77 (1.67)	0.23	1	0					
f025	107.415 (0.015)	9309.69 (1.30)	0.39	2	0		58		-0.05	
f026	108.085 (0.010)	9251.98 (0.86)	0.29	1	-1	32		0.06		
f027	111.155 (0.036)	8996.45 (2.93)	0.32	2	-1		56		-0.10	0.182
f028	111.337 (0.030)	8981.74 (2.45)	0.35	2	0	31	56	0.05	-0.19	0.566
f029	111.903 (0.005)	8936.31 (0.42)	0.48	2	2		56		-0.49	
f030	114.062 (0.009)	8767.16 (0.68)	1.00	2	-1		54		0.41	0.307
f031	114.369 (0.006)	8743.63 (0.49)	0.92	2	0		54		0.25	0.291
f032 [†]	114.660 (0.014)	8721.44 (1.05)	1.41	2	1		54		0.11	
f033	116.204 (0.004)	8605.56 (0.31)	0.19							
f034	118.624 (0.008)	8430.00 (0.56)	0.27	2	-2		52		0.21	0.242
f035 [†] *	118.866 (0.012)	8412.83 (0.82)	1.31	2	-1		52		0.09	0.218
f036	119.084 (0.010)	8397.43 (0.71)	0.43	2	-		52		-0.01	0.278
f037	119.362 (0.013)	8377.88 (0.91)	0.26	2	1		52		-0.14	0.229
f038	119.591 (0.007)	8361.83 (0.49)	0.23	2	2		52		-0.24	
f039	122.260 (0.120)	8179.29 (8.02)	0.22	1	-1	28		0.04		
f040 [†]	126.095 (0.023)	7930.53 (1.45)	1.15	2	0		49		-0.05	

TABLE 1—*Continued*

ID	Freq. μHz	Period sec.	Amp. ppt	ℓ ...	m ...	$n_{\ell=1}$...	$n_{\ell=2}$...	$(\frac{\Delta P}{P})_{\ell=1}$...	$(\frac{\Delta P}{P})_{\ell=2}$...	δf μHz
f041	130.993 (0.007)	7634.00 (0.41)	0.19	1	0	26	47	-0.01	0.01	0.116
f042	131.109 (0.015)	7627.24 (0.87)	0.18	1	1	26	47	-0.03	-0.03	
f043	135.606 (0.013)	7374.30 (0.71)	0.35	1	-1	25		0.02		0.104
f044 ^{†*}	135.710 (0.017)	7368.65 (0.91)	0.35	1	0	25		-0.01		0.112
f045	135.822 (0.015)	7362.58 (0.81)	0.48	1	1	25		-0.03		
f046	140.530 (0.045)	7115.92 (2.28)	1.28	2	-1		43		0.63	0.3
f047	140.830 (0.045)	7100.76 (2.27)	1.22	2	0		43		0.53	0.163
f048 [†]	140.993 (0.012)	7092.55 (0.63)	2.29	2	1	24	43	-0.04	0.48	
f049	142.521 (0.007)	7016.51 (0.33)	0.30	2	1		43		-0.02	
f050	144.362 (0.014)	6927.03 (0.66)	0.21							0.752
f051	145.114 (0.005)	6891.13 (0.24)	0.20	2	-2		42		0.16	0.299
f052	145.413 (0.007)	6876.96 (0.33)	0.26	2	-1		42		0.07	0.283
f053	145.696 (0.024)	6863.61 (1.14)	0.45	2	0		42		-0.02	0.065
f054	145.761 (0.014)	6860.55 (0.67)	0.45	2			42		-0.04	
f055	146.344 (0.012)	6833.21 (0.58)	0.29							0.186
f056	146.530 (0.015)	6824.54 (0.70)	0.40	1	-1	23		-0.05		0.107
f057	146.637 (0.009)	6819.56 (0.40)	0.43	1	0	23		-0.07		
f058	148.156 (0.009)	6749.64 (0.41)	0.19							
f059	151.942 (0.015)	6581.46 (0.66)	0.38	1	0	22		0.04		1.739
f060	153.681 (0.021)	6506.99 (0.90)	0.20							
f061	156.244 (0.009)	6400.25 (0.37)	0.27	2	0		39		-0.04	
f062	157.706 (0.009)	6340.91 (0.36)	0.18							
f063 [*]	158.845 (0.036)	6295.45 (1.44)	1.51	1	-1	21		-0.03		0.107
f064	158.952 (0.009)	6291.21 (0.36)	0.67	1	0	21		-0.05		0.134
f065 [†]	159.086 (0.011)	6285.91 (0.43)	0.71	1	1	21		-0.07		
f066 [†]	159.731 (0.009)	6260.53 (0.35)	0.23	2			38		0.05	
f067	165.633 (0.007)	6037.44 (0.26)	0.42	1	-1	20		0.00		0.142
f068	165.775 (0.025)	6032.27 (0.91)	0.25	1	0	20		-0.02		0.139
f069	165.914 (0.006)	6027.22 (0.20)	0.35	1	1	20		-0.04		
f070 [†]	167.786 (0.006)	5959.97 (0.21)	0.26	2	-1		36		0.09	0.229
f071	168.015 (0.017)	5951.85 (0.60)	0.26	2	0		36		0.03	0.202
f072	168.217 (0.007)	5944.70 (0.25)	0.23	2	1		36		-0.01	0.273
f073	168.490 (0.035)	5935.07 (1.23)	0.17	2	2		36		-0.08	
f074 [†]	171.908 (0.013)	5817.06 (0.43)	0.89							0.232
f075	172.140 (0.030)	5809.23 (1.01)	0.70							0.189
f076	172.329 (0.017)	5802.85 (0.56)	0.49	2	-1		35		0.06	0.2
f077	172.529 (0.011)	5796.13 (0.39)	0.68	2	0		35		0.02	0.211
f078	172.740 (0.039)	5789.05 (1.31)	0.25	2	1		35		-0.03	0.28
f079	173.020 (0.019)	5779.68 (0.63)	0.41	2	2		35		-0.09	0.161
f080	173.181 (0.005)	5774.31 (0.18)	0.41	1	0	19		0.01		0.138

TABLE 1—*Continued*

ID	Freq. μHz	Period sec.	Amp. ppt	ℓ ...	m ...	$n_{\ell=1}$...	$n_{\ell=2}$...	$(\frac{\Delta P}{P})_{\ell=1}$...	$(\frac{\Delta P}{P})_{\ell=2}$...	δf μHz
f081	173.319 (0.016)	5769.71 (0.52)	1.39	2	-2		35		-0.16	
f082	177.871 (0.025)	5622.05 (0.78)	0.24	2			34		-0.12	
f083	178.930 (0.009)	5588.78 (0.28)	0.19	1	0	18		0.31		0.088
f084	179.018 (0.004)	5586.03 (0.14)	0.20	1	1	18		0.30		
f085	180.763 (0.012)	5532.11 (0.37)	0.45							0.261
f086 [†]	181.024 (0.022)	5524.13 (0.68)	0.96							0.528
f087	181.552 (0.006)	5508.06 (0.18)	0.20	1	1	18		0.01		0.508
f088	182.060 (0.007)	5492.69 (0.21)	0.24	2	-2		33		0.04	0.54
f089	182.600 (0.017)	5476.45 (0.51)	0.25	2	1		33		-0.07	0.652
f090	183.252 (0.021)	5456.97 (0.62)	0.47							
f091	187.796 (0.023)	5324.93 (0.65)	0.45	2	-1		32		-0.06	0.246
f092	188.042 (0.010)	5317.96 (0.29)	0.29	2	0		32		-0.10	0.203
f093	188.245 (0.010)	5312.23 (0.29)	0.19	2	1		32		-0.14	0.233
f094	188.478 (0.004)	5305.66 (0.12)	0.15	2	2		32		-0.18	
f095	189.570 (0.006)	5275.10 (0.17)	1.53	1		17		0.14		
f096	193.031 (0.010)	5180.52 (0.27)	0.20	2	-2		31		0.00	0.202
f097	193.233 (0.023)	5175.10 (0.62)	0.20	2	-1		31		-0.04	0.205
f098	193.438 (0.008)	5169.62 (0.22)	0.21	2	0		31		-0.07	0.228
f099*	193.666 (0.007)	5163.53 (0.19)	0.22	2	1		31		-0.11	
f100	198.960 (0.005)	5026.14 (0.13)	0.17	2	-1		30		-0.01	0.71
f101	199.670 (0.005)	5008.26 (0.13)	0.18	2	2		30		-0.12	
f102	204.698 (0.006)	4885.25 (0.14)	0.18	2	-2		29		0.07	0.343
f103 [†]	205.041 (0.007)	4877.07 (0.18)	0.22	2	-1		29		0.02	0.332
f104	205.373 (0.033)	4869.19 (0.77)	0.25	2	0		29		-0.03	0.437
f105	205.810 (0.006)	4858.85 (0.14)	0.20	2	2		29		-0.10	0.739
f106	206.549 (0.005)	4841.47 (0.13)	0.23							
f107	211.620 (0.007)	4725.45 (0.17)	0.43	2	-1		28		0.03	0.264
f108 ^{†*}	211.884 (0.006)	4719.56 (0.14)	3.30	2	0		28		-0.01	0.321
f109	212.205 (0.007)	4712.42 (0.15)	0.52	2	1		28		-0.06	0.282
f110 [†]	212.487 (0.010)	4706.17 (0.22)	0.48	2	2		28		-0.10	0.562
f111	213.049 (0.017)	4693.76 (0.37)	0.70	1		15		-0.05		
f112 [†]	217.834 (0.011)	4590.65 (0.22)	0.47	2	-2		27		0.15	0.256
f113	218.090 (0.015)	4585.26 (0.32)	0.87	2	-1		27		0.11	0.187
f114*	218.277 (0.021)	4581.33 (0.44)	1.14	2	0		27		0.09	0.223
f115 [†]	218.500 (0.037)	4576.66 (0.77)	0.78	2	1		27		0.06	0.253
f116	218.753 (0.007)	4571.37 (0.15)	0.45	2	2		27		0.02	
f117	221.981 (0.032)	4504.89 (0.65)	0.21							3.221
f118	225.202 (0.005)	4440.46 (0.10)	0.58	1	0	14		0.00		
f119	227.151 (0.011)	4402.36 (0.21)	0.36	2			26		-0.08	
f120	234.423 (0.007)	4265.79 (0.13)	0.42	2	-1		25		0.03	0.176

TABLE 1—*Continued*

ID	Freq. μHz	Period sec.	Amp. ppt	ℓ ...	m ...	$n_{\ell=1}$...	$n_{\ell=2}$...	$(\frac{\Delta P}{P})_{\ell=1}$...	$(\frac{\Delta P}{P})_{\ell=2}$...	δf μHz
f121 [†]	234.599 (0.010)	4262.59 (0.19)	0.44	2	0		25		0.01	0.209
f122	234.808 (0.015)	4258.80 (0.27)	0.30	2	1		25		-0.02	0.195
f123	235.003 (0.006)	4255.26 (0.10)	0.28	2	2		25		-0.04	
f124	239.422 (0.005)	4176.73 (0.08)	0.27	1	0	13		0.01		
f125	252.987 (0.025)	3952.77 (0.39)	1.79	2	-2		23		-0.01	0.207
f126 ^{†*}	253.194 (0.023)	3949.54 (0.36)	1.21	2	-1		23		-0.03	0.188
f127	253.382 (0.012)	3946.61 (0.19)	0.53	2	0		23		-0.05	0.199
f128	253.581 (0.015)	3943.51 (0.24)	0.28	2	1		23		-0.07	0.216
f129	253.797 (0.008)	3940.16 (0.12)	0.20	2	2		23		-0.09	
f130 [†]	255.686 (0.006)	3911.05 (0.09)	7.11	1	0	12		0.01		
f131	262.151 (0.008)	3814.60 (0.11)	0.50							0.099
f132	262.250 (0.004)	3813.16 (0.06)	0.36	2	-2		22		0.08	0.215
f133 [†]	262.465 (0.008)	3810.03 (0.12)	0.35	2	-1		22		0.06	0.779
f134 [†]	263.244 (0.010)	3798.76 (0.15)	0.59	2	2		22		-0.02	
f135	274.455 (0.016)	3643.58 (0.21)	0.18	2	-2	11	21	0.01	-0.03	0.245
f136	274.700 (0.009)	3640.33 (0.12)	0.28	2	-1	11	21	0.00	-0.05	0.433
f137 [†]	275.133 (0.021)	3634.61 (0.27)	0.59	2	1		21		-0.09	0.223
f138	275.356 (0.009)	3631.66 (0.12)	0.44	2	2		21		-0.11	
f139	286.171 (0.005)	3494.41 (0.06)	0.23	2	-1		20		0.00	0.255
f140	286.426 (0.007)	3491.30 (0.09)	0.17	2	0		20		-0.02	0.481
f141	286.907 (0.007)	3485.45 (0.09)	0.32	2	2		20		-0.06	
f142	298.961 (0.004)	3344.92 (0.05)	0.23	2	-1		19		0.02	0.341
f143 [*]	299.302 (0.005)	3341.11 (0.05)	0.42	2	0		19		0.00	
f144	312.217 (0.010)	3202.90 (0.10)	0.19	2	-1		18		0.09	0.241
f145	312.458 (0.014)	3200.43 (0.14)	0.16	2	0		18		0.08	0.241
f146 [*]	312.699 (0.007)	3197.96 (0.07)	0.13	2	2		18		0.06	0.245
f147	312.944 (0.007)	3195.46 (0.07)	0.16	2	1		18		0.05	
f148	346.949 (0.015)	2882.27 (0.12)	0.19	2			16		0.00	
f149	358.701 (0.005)	2787.84 (0.04)	0.25							
f150 [†]	366.419 (0.005)	2729.12 (0.04)	1.05	2			15		0.00	
f151 [†]	389.015 (0.005)	2570.59 (0.03)	0.68	1 or 2		7	14	-0.02	-0.03	
f152	427.770 (0.012)	2337.70 (0.07)	0.16							0.257
f153	428.027 (0.013)	2336.30 (0.07)	0.20	1	0	6		0.10		
f154 [†]	441.507 (0.005)	2264.97 (0.03)	0.79	2			12		-0.03	
f155	459.762 (0.042)	2175.04 (0.20)	0.17	2	2		11		0.39	0.234
f156	459.996 (0.009)	2173.93 (0.04)	0.38	2	-1		11		0.38	0.465
f157	460.461 (0.007)	2171.74 (0.03)	0.21	2	1		11		0.36	
f158 [*]	565.893 (0.016)	1767.12 (0.05)	0.21	4	-4					0.501
f159 [†]	566.394 (0.006)	1765.56 (0.02)	1.21	4	-2					0.526
f160	566.920 (0.010)	1763.92 (0.03)	0.44	4	0					0.538

TABLE 1—*Continued*

ID	Freq. μHz	Period sec.	Amp. ppt	ℓ ...	m ...	$n_{\ell=1}$...	$n_{\ell=2}$...	$(\frac{\Delta P}{P})_{\ell=1}$...	$(\frac{\Delta P}{P})_{\ell=2}$...	δf μHz
f161	567.458 (0.014)	1762.24 (0.04)	0.25	4	2					0.319
f162	567.777 (0.010)	1761.25 (0.03)	0.25	4	4					
f163	614.605 (0.009)	1627.06 (0.02)	0.21							
f164	662.979 (0.028)	1508.34 (0.06)	0.16	4	-3					0.251
f165	663.230 (0.014)	1507.77 (0.03)	0.19	4	-2					0.219
f166	663.449 (0.007)	1507.27 (0.02)	0.16	4	-1					0.213
f167 [†]	663.662 (0.029)	1506.79 (0.07)	0.20	4	0					0.778
f168	664.440 (0.021)	1505.03 (0.05)	0.17	4	3					0.36
f169	664.800 (0.015)	1504.21 (0.03)	0.16	4	4					
f170 [†]	719.582 (0.020)	1389.70 (0.04)	0.20							0.311
f171	719.893 (0.008)	1389.10 (0.02)	0.18							
f172	743.009 (0.010)	1345.88 (0.02)	0.22	2	-1		6		-0.02	0.332
f173	743.341 (0.012)	1345.28 (0.02)	0.25	2	0		6		-0.03	0.232
f174 [†]	743.573 (0.007)	1344.86 (0.01)	0.25	2	1		6		-0.03	
f175 [†]	744.545 (0.010)	1343.10 (0.02)	0.23				6		-0.04	
f176	748.392 (0.008)	1336.20 (0.01)	0.45	2	-2		6		-0.09	0.307
f177	748.699 (0.009)	1335.65 (0.02)	1.19	2	-1		6		-0.09	0.315
f178	749.014 (0.012)	1335.09 (0.02)	0.56	2	0		6		-0.10	0.32
f179 [†]	749.334 (0.017)	1334.52 (0.03)	0.75	2	1		6		-0.10	0.38
f180	749.714 (0.038)	1333.84 (0.07)	0.75	2	2		6		-0.10	
f181	773.069 (0.010)	1293.55 (0.02)	0.32	2	-1		6		-0.37	0.366
f182	773.435 (0.006)	1292.93 (0.01)	0.43	2	0		6		-0.37	0.385
f183	773.820 (0.011)	1292.29 (0.02)	0.50	2	1		6		-0.37	0.329
f184*	774.149 (0.013)	1291.74 (0.02)	0.22							0.313
f185	774.462 (0.033)	1291.22 (0.06)	0.28							0.214
f186 [†]	774.676 (0.024)	1290.86 (0.04)	0.41							0.12
f187	774.796 (0.016)	1290.66 (0.03)	0.43							0.452
f188	775.248 (0.009)	1289.91 (0.01)	0.31							
f189	777.390 (0.040)	1286.36 (0.07)	0.50							0.623
f190	778.013 (0.008)	1285.326 (0.013)	0.17	4	-4					0.282
f191	778.295 (0.008)	1284.860 (0.013)	0.15	4	-3					0.299
f192	778.594 (0.030)	1284.366 (0.049)	0.14	4	-2					0.261
f193	778.855 (0.005)	1283.936 (0.009)	0.25	4	-1					0.283
f194	779.138 (0.007)	1283.470 (0.011)	0.24	4	0					0.285
f195	779.423 (0.008)	1283.000 (0.014)	0.25	4	1					0.297
f196	779.720 (0.025)	1282.512 (0.041)	0.25	4	2					0.55
f197	780.270 (0.007)	1281.608 (0.011)	0.12	4	4					
f198	823.716 (0.011)	1214.011 (0.016)	0.20							5.933
f199	829.649 (0.006)	1205.329 (0.008)	0.20	2			5		0.06	
f200	887.122 (0.008)	1127.241 (0.010)	0.17							

TABLE 1—*Continued*

ID	Freq. μHz	Period sec.	Amp. ppt	ℓ ...	m ...	$n_{\ell=1}$...	$n_{\ell=2}$...	$(\frac{\Delta P}{P})_{\ell=1}$...	$(\frac{\Delta P}{P})_{\ell=2}$...	δf μHz
f201	892.890 (0.007)	1119.959 (0.009)	0.23							0.612
f202	893.502 (0.008)	1119.192 (0.010)	0.18							0.291
f203 [†]	893.793 (0.030)	1118.827 (0.038)	0.19							
f204	931.652 (0.019)	1073.362 (0.022)	0.20							0.327
f205	931.979 (0.006)	1072.986 (0.006)	0.20							0.365
f206	932.344 (0.037)	1072.565 (0.043)	0.43							0.23
f207 [†]	932.574 (0.020)	1072.301 (0.023)	0.47							0.42
f208*	932.994 (0.016)	1071.818 (0.019)	0.62							
f209	969.427 (0.010)	1031.537 (0.011)	0.27	2			4		-0.08	0.463
f210	969.890 (0.010)	1031.045 (0.011)	0.25	2			4		-0.08	
f211 [†]	1002.650 (0.008)	997.357 (0.008)	0.26							0.272
f212	1002.922 (0.043)	997.087 (0.043)	0.25							
f213	1012.924 (0.008)	987.241 (0.008)	0.24	9	-9					0.220
f214	1013.144 (0.063)	987.027 (0.061)	0.18	9	-8					0.478
f215	1013.622 (0.030)	986.561 (0.029)	0.18	9	-6					0.496
f216	1014.118 (0.011)	986.079 (0.011)	0.23	9	-4					0.474
f217	1014.592 (0.025)	985.618 (0.024)	0.33	9	-2					0.195
t218	1014.787 (0.085)	985.428 (0.083)	0.16	9	-1					0.225
f219	1015.012 (0.035)	985.210 (0.034)	0.34	9	0					0.208
f220	1015.220 (0.015)	985.008 (0.015)	0.18	9	1					0.243
f221	1015.463 (0.018)	984.772 (0.017)	0.50	9	2					0.417
f222 [†]	1015.880 (0.015)	984.368 (0.015)	0.50	9	4					0.397
f223	1016.277 (0.035)	983.984 (0.034)	0.74	9	6					0.430
f224	1016.711 (0.015)	983.564 (0.015)	0.45	9	8					0.190
f225	1016.901 (0.025)	983.380 (0.024)	0.58	9	9					
f226	1133.916 (0.006)	881.900 (0.005)	0.17							1.815
f227	1135.731 (0.007)	880.490 (0.005)	0.17							
f228	1508.306 (0.020)	662.995 (0.009)	0.19							0.066
f229	1508.372 (0.020)	662.966 (0.009)	0.22							
f230	1518.291 (0.010)	658.635 (0.004)	0.17							
f231	1573.084 (0.005)	635.694 (0.002)	0.18							
f232	1598.436 (0.016)	625.612 (0.006)	0.20							
f233	1650.710 (0.007)	605.800 (0.002)	0.23							
f234	1666.173 (0.007)	600.178 (0.003)	0.18							
f235	1696.132 (0.007)	589.577 (0.002)	0.24							
f236	1756.324 (0.032)	569.371 (0.010)	0.20							
f237	1846.183 (0.008)	541.658 (0.002)	0.18							
f238 [†]	2767.518 (0.008)	361.335 (0.001)	2.82	0	0					
f239 [†]	2782.454 (0.033)	359.395 (0.004)	0.45	1	-1					0.747
t240	2783.201 (0.008)	359.299 (0.001)	0.13	1	0					0.726

TABLE 1—*Continued*

ID	Freq. μHz	Period sec.	Amp. ppt	ℓ ...	m ...	$n_{\ell=1}$...	$n_{\ell=2}$...	$(\frac{\Delta P}{P})_{\ell=1}$...	$(\frac{\Delta P}{P})_{\ell=2}$...	δf μHz
f241	2783.927 (0.014)	359.205 (0.002)	0.20	1	1					
t242	2814.226 (0.037)	355.337 (0.005)	0.13	2	-2					0.779
t243	2815.005 (0.030)	355.239 (0.004)	0.13	2	-1					0.73
f244	2815.735 (0.008)	355.147 (0.001)	0.18	2	0					0.714
f245	2816.449 (0.025)	355.057 (0.003)	0.65	2	1					0.795
t246	2817.244 (0.031)	354.957 (0.004)	0.14	2	2					
f247	3686.925 (0.009)	271.229 (0.001)	0.16							0.422
f248	3687.347 (0.030)	271.198 (0.002)	0.15							
f249	3700.778 (0.017)	270.213 (0.001)	0.17							1.956
f250 [†]	3702.734 (0.088)	270.071 (0.006)	0.17							1.025
f251	3703.759 (0.034)	269.996 (0.002)	0.17							